1 # Synthesis and Characterization of Erbium Trioxide
2 # Nanoparticles as Photo-Catalytic for Degradation of
3 # Methyl Orange Dye

5 Rifat Mohammed Dakhil[1], Tayser Sumer Gaaz[2], Ahmed Al-Amiery[3,*] Mohd S. Takriff[3] and

6 Abdul Amir H. Kadhum[3,]

8 1 Technical College Basra, Southern Technical University, Iraq

9 2 Department of Machinery Equipment Engineering Techniques, Technical College Al-

10 Musaib, Al-Furat Al Awsat Technical University, Al-Musaib, Babil 51009, Iraq

11 3 Department of Chemical & Process Engineering, Faculty of Engineering & Built

12 Environment, Universiti Kebangsaan Malaysia, Bangi, Selangor 43600, Malaysia

14 * Correspondence: dr.ahmed1975@gmail.com

15 **ABSTRACT**

16 The present work focuses on the photo-catalytic degradation of methyl orange (MO) on

17 Erbium trioxide nanoparticles "Er_2O_3 NPs". In this study, Er_2O_3 nanoparticles were

18 synthesized and fully characterized via various techniques including; XRD diffraction, UV-

19 Vis spectroscopy and SEM techniques. The results revealed that, the photo-catalytic activity

20 of the prepared Er_2O_3 NPs towards methyl orange (MB) photo-degradation was manifested.

21 The optimum efficiency obtained was 16%.

23 **Keywords:** methyl orange; Er_2O_3; Photo-catalytic; XRD; SEM Nomenclature

24 **1 Introduction**

25 One of the sources of water contamination was the wastewater generated from textile-plants

26 employing various dyestuffs (Khataee and Kasiri, 2010; Barbe et al., 1997). Various chemical

27 and physical in addition to biological changes for dyes could occur that consume dissolved

28 oxygen in the water bodies. Moreover, dyes have high toxicity which endangers aquatic life

29 (Khataee et al., 2009; Ruiz et al., 2004). The various traditional techniques employed for the

30 processing of pollutants textile dyes in water involve different chemical, biological and/or

31 physical techniques. Photo-catalytic degradation was demonstrate as a promising technique for

32 processing of pollutions that occur due to organic and/or inorganic compounds. The approach,

33   as a means of removal of persistent water contaminants like dyes and pesticides was attracted

34   recently the attention of numerous investigators (Xu et al., 2014; Chen et al., 2014; Liu et al.,

35   2014). Considerable of these researchers were used suspension (aqueous) of semi-conductors

36   irradiated by UV-light to photo-degrade the pollutants (Daneshvar et al., 2007). The

37   accomplishment of a semi-conductor photo-catalyst was strongly connected with the electronic

38   structure of it (Daneshvar et al., 2007; Boppella et al., 2013; Xiao et al., 2012; Alenezi et al.,

39   2013). It was established that the photo-catalytic degradation of organic ions or organic

40   molecules in solution are launched by photo-generated holes in valence band with electrons in

41   the conduction band of the semi-conductor photo-catalyst. The generated holes have high

42   oxidative potential that permits a direct oxidation of organic ions or organic molecules to

43   reactive intermediates. Moreover, radicals are reactive species that may help in organic

44   substrate degradation. Methyl orange as in Fig. 1, is a scale of acidity utilized in titration due

45   to its clear and distinct color difference at various pH values. Methyl orange demonstrates pink

46   colour in acidic solution and yellow colour in basic solution. Due to it variations colour at the

47   pH of a mid-strength acid, it is ordinarily utilized in titration for acid solutions. Unlike a global

48   indicator, methyl orange does not have a full spectrum of colour variation, but it has a sharp

49   end (Khodja et al., 2001; Sandberg et al., 1972).

50

51   Fig. 1

52

53   Generally, MO utilized monoazo dye in laboratory tests, textiles and different commercial

54   products and has to be eliminate from water because of its toxicity (Mittal et al., 2007; Chen et

55   al., 2010). Mittal et al. (Mittal et al., 2007) searched the eliminate and recovery of MO from

56   wastewaters employing waste materials. Chen and his co-workers (Chen et al., 2010) examined

57   the equilibrium and kinetic aspects of MO adsorption on activated carbon derived from

58   Phragmites austral is. Jiang and other researchers (Jiang et al., 2012) investigated the removal

59   of MO from solutions through Maghemite-Chitosan NPs. Therefore, there is a need to develop

60   a novel treatment method that is more effective in eliminating dyes from the wastewater. The

61   objective and novelty of the present work is to study the factors effecting on photo-catalytic oxidation

62   process of methyl orange dye using the synthesized erbium trioxide Nanoparticles such as

63   concentration, illumination time and amount of catalyst loaded used in photo-catalytic process. In

64   this investigation, we searched the photo-catalytic degradation of MO on Er_2O_3 NPs.

65

66

67   **2   Experimental**

68   2.1 Materials

69   All materials used in this work were supplied from Fluka Company, and were used without
70   further purification.

71   2.2 Synthesis of Er_2O_3 NPs

72   Erbium oxide nanoparticles (Er_2O_3 NPs) had been synthesized by dissolving of ascorbic acid
73   (1 g) and of sodium fluoride (0.063 g) in distilled water (10 mL). Adjusted the pH solution to
74   four by adding drops of ammonium hydroxide solution. The resulting solution was heated to
75   70 ℃ for 20 min. An alcoholic solution of Erbium nitrate (2.5 g in 4 mL) had been added to
76   the above solution and continuous stirring 2 hr. At room temperature. Centrifuged and washed
77   the precipitate several times with de-ionized water dried in air for 24 hr under vacuum. The
78   precipitate, then calculated at 800 ℃ for 3 hr.

79   2.3 Sample Preparation

80   Er_2O_3 nanoparticles were prepared as the catalyst of 0.1 g diluted in 100 mL methanol). Erbium
81   oxide Er_2O_3 and methyl orange (MO) were weighed by using sensitive balance. MO as a dye
82   often used for catalytic tests (0.05 g diluted with 500 mL methanol).

83   2.4 Photo-Catalytic Setup

84   The photo-catalytic set-up consists of UV- source as a lamp (6 watt) of cylindrical shape 22
85   cm body length and 16 cm arc length of cylindrical shape, which was used as a photo source.
86   This was used as a photo source. This lamp was positioned in a container of the sample (mixture
87   of Er_2O_3 NPs and MO) and then placed on magnetic stirrer (to mix and disperse solutions result
88   of high speeds and long time to prepare it solutions) (Chen et al., 2014).

89   2.5 Methods

90   2.5.1   Irradiation Time Effect

91   The Mixture of Er_2O_3 NPs and MO was placed on magnetic stirrer and the temperature was
92   fixed at 25 ℃. The UV-lamp was switched on inside the sample container. Different irradiation
93   time (1, 2, 3, 4 and 5 hr) were employed. The photo degradation measured after each hour. The
94   samples were examined by UV-spectrometer to measure the absorbance of all sample.

95   2.5.2   Dye Concentration Effect

96   Different concentrations of the MO were used in the range of (0.1, 0.2, 0.5, 1, 1.5, 2) wt.% and

97   0.1 wt.% from Er_2O_3 NPs. The samples withdrawn from the mixture without photo catalysts

98   and after 15 minute for each concentration of MO. The samples were examined by UV-visible

99   spectrophotometer to measure the optical absorbance.

100   2.5.3   Scanning Electron Microscopy (SEM)

101   The morphology of the nanoparticles of Erbium oxide nanoparticles was studied by SEM. It

102   was recorded on the JEOL JSM-6390LV SEM fitted with secondary electron detector.

103   2.5.4   X-ray diffraction (XRD)

104   The crystallinity of Er_2O_3 powder was studied by X-ray diffraction (XRD) technique.

105   **3   Results and Discussion**

106   To improve the photo-degradation efficiency of methyl orange dye, erbium trioxide nanoparticles
107   were used as a common strategy. Erbium trioxide nanoparticles were ready to synthesis and cheap.
108   Various types of nano-metal have been used in the previous studies, including anionic dopants,
109   cationic dopants, rare-earth dopants, and codopants (Samadi et al., 2014). Besides, many studies
110   have shown that coupling with other semiconductors, such as CdO (Liu et al., 2014), CeO2 (Uddin
111   et al., 2012)], SnO2,TiO2 (Pant et al., 2012), graphene oxide (GO) (Dai et al., 2014), and reduced
112   grapheme oxide (RGO) (Zhou et al., 2012), is a feasible approach to enhance the photodegradation
113   efficiency.

114   3.1 Absences of Sunlight

115   The results had been discussed with/without sunlight as shown in Figs. 2 and 3. Fig. 2

116   demonstrates the relation between absorbance and time of photo-catalytic without sunlight

117   radiation. The increasing of time of photo-degradation up to 3.0 hr, leads to that the absorbance

118   values will raise, due to the degradation process organic dye. This attitude harmonize with

119   Lazar et al. (Lazar et al., 2012). Fig. 3 elucidate the absorption of Er_2O_3 spectrum in absence

120   of sun light (SL), that could be shown that the minimum absorption occur at wavelength range

121   of (324-489 nm) for various irradiative time.

122

123   Fig. 2

124

125   Fig. 3 shows the absorption spectrum of Er_2O_3 nanoparticles without SL. One can be

126   shown that the minimum absorption take place at the range of wavelength (450-600 nm) for

127   different irradiative time. A transmission spectrum has maximum intensities at wavelengths

128   where the absorption is weakest because more light is transmitted through the sample. An

129 absorption spectrum has maximum intensities at wavelengths where the absorption is strongest.

130 When sample molecules are exposed to light having an energy that matches a possible

131 electronic transition within the molecule, some of the light energy will be absorbed as the

132 electron is promoted to a higher energy orbital. An optical spectrometer records the

133 wavelengths at which absorption occurs, together with the degree of absorption at each

134 wavelength. Absorbance usually ranges from 0 to 3.5, and is precisely defined in context with

135 spectrometer operation.

136

137   Fig. 3

138 3.2 In presence of SL

139 Fig. 4 shows the photo-catalytic degradation of diazocompounds irradiated under sunlight in

140 the presence of Er_2O_3 nanoparticles. The presence of Er_2O_3 nanoparticles was investigated as

141 a very important factor for improvement the degradation process. Higher efficiency of

142 degradation was found within 4.0 hr, of irradiation time and considering the optimum loading

143 of catalyst. After 4.0 hr, of irradiation time with Er_2O_3 nanoparticles, can be shown other peak

144 at irradiation time of 5.0 hr, when we carried out a comparison between the absorbance values

145 at 5 hr. with Fig. 2 and without sunlight can be conclude the improvement in phenolic

146 compound degradation when taken into account the role of sunlight.

147

148   Fig. 4

149

150   The rate of reaction increases and maximum rates were getting after four hour as shown in

151 Fig. 5. It may be explained on the basis that the operation time of UV source was increased,

152 the number of photons per unit area incident on the sample also increased, resulting in high

153 rate of degradation in the mixture of Erbium oxide and MO Leads to increase the absorption

154 value.

155

156   Fig. 5

157 3.3 Impact of Methylene Blue Concentration

158 3.3.1   Concentration of MO Effects without Irradiation

159 The increasing in the dye concentration leads to increases of absorbance. The maximum change

160 of absorbance increasing was noticed when the concentration changed from 0.5 wt.% to 1wt.%

161 as shown in Fig. 6. The degradation efficiency of MO was analyzed using UV-Vis

162 spectrometer. Peaks were observed to be present between 450 and 600 nm, which was

163 indicative of the degradation of MO. According to Beer-Lambert Law, MO concentration is

164 directly proportional to its absorbance (Ramli et al., 2014).

165 ### 3.3.2 Concentration of MO Effects with Irradiation

166 When MO concentration increased leads to the value of absorbance was increased after 15 min

167 from irradiation. Maximum increasing in absorbance notice when changed the concentration

168 at the period (0.5-1.0) wt.% as shown in Fig. 6. This might be elucidated base on the increasing

169 of dye concentrations that leads to the reaction average increases as additional, molecules.

170 When increased the dye (3.0-5.0) wt.% the value of absorbance remains constant at 4.51 wt.%

171 cause reaction retardation because of the increasing in number of collisions between dye

172 molecules whereas, collisions between dye and salt decrease. As a conclusion, proportion of

173 reaction was decrease (Karunakaran et al., 2004; Pandey et al., 2015). The main rate of

174 degradation exists in the region near irradiated side where the intensity of irradiation was much

175 higher than in the other sides. Thus, dye with higher concentration, the degradation technique

176 decreases at sufficiently long distances from the light source or the reaction zone because of

177 retardation in the penetration of light.

178

179 Fig. 6

180 ### 3.4 SEM Results

181 The SEM micrographs of synthesized samples are shown in Figs. 7, 8, 9 and 10, this Figs. show

182 the distribution and the morphology of Er_2O_3 nanoparticles. The average size of the

183 nanoparticles was found to be (~16 nm) and appeared to be uniform.

184

185 Fig. 7

186

187 Fig. 8

188

189 Fig. 9

190

191 Fig. 10

192   3.5 XRD Results

193   XRD was used to clarify the Er_2O_3 nanoparticles phase formation. All the reflections were well

194   indexed to cubic phase of Er_2O_3 nanoparticles and can be seen from Fig. 11, XRD parameter

195   of Er_2O_3 nanoparticles show in Table 1 with a space group of I 21 3 (199) and cell parameters

196   of a=10.5400 Å. The excellent crystallinity and absence of impurities can be inferred because

197   of sharpness and exact number of peaks in the XRD pattern. Additionally, it indicates that the

198   product is a single phase. XRD was used to clarify the Er_2O_3 nanoparticles phase formation.

199   All the reflections were well indexed to cubic phase of Er_2O_3 nanoparticles, the average

200   crystallite size of Er_2O_3 nanoparticles is found to be 16 nm.

201

202   Fig. 11

203   Table 1

204

205   **4   Conclusion**

206   Nanoparticles of Er_2O_3 under SL improvement the effectiveness degradation diazomium

207   compounds for methyl orange or in other words removal of mixture polluted by methyl orange.

208   The photo catalytic activity under UV and light illumination, components for the enhanced

209   photo synergist reactivity of the Er_2O_3. The Er_2O_3 nanoparticles have stage and it is ready to

210   ingest a high measure of photo catalytic in the obvious light area, driving adequately

211   photochemical degradation responses. Maximum increasing of absorbance was noticed when

212   the concentration of MO increased from 0.5 wt.% to 1wt.% and this behavior leads to

213   increasing degradation of MO up to 14 % for Er_2O_3 catalyst. XRD measurements show that the

214   structure of Er_2O_3 nanoparticles was Cubic, the average crystallite size of Er_2O_3 nanoparticles

215   is found to be 16 nm.

216   **Acknowledgments**

217   The authors gratefully acknowledge the UKM-YSD Chair on Sustainable Development for the

218   Grant 020–2017 'Malaysia' for supporting this work.

219   **References**

220   Alenezi MR, Alshammari AS, Jayawardena KI, et al. (2013), *The Journal of Physical*

221   Alenezi, M. R., Alshammari, A. S., Jayawardena, K. I., Beliatis, M. J., Henley, S. J., &

222   Silva, S.: Role of the exposed polar facets in the performance of thermally and UV

223   activated ZnO nanostructured gas sensors, The Journal of Physical Chemistry C,
224   117(34), 17850-17858, https://pubs.acs.org/doi/abs/10.1021/jp4061895, 2013.

225

226   Barbe, C. J., Arendse, F., Comte, P., Jirousek, M., Lenzmann, F., Shklover, V., &
227   Grätzel,
228   M.: Nanocrystalline titanium oxide electrodes for photovoltaic applications, Journal
229   of the American Ceramic Society, 80(12), 3157-3171,
230   https://onlinelibrary.wiley.com/doi/abs/10.1111/j.1151-2916.1997.tb03245.x, 1997.

231

232   Boppella, R., Anjaneyulu, K., Basak, P., & Manorama, S. V.: Facile synthesis of face
233   oriented ZnO crystals: tunable polar facets and shape induced enhanced photocatalytic
234   performance, The Journal of Physical Chemistry C, 117(9), 4597-4605,
235   https://pubs.acs.org/doi/10.1021/jp311443s, 2013.

236

237   Chen, J., Li, S., Ma, S., & Wang, X.: Polar Fuzzy Sets: An Extension of Bipolar Fuzzy
238   Sets, The Scientific World Journal, 2014,
239   https://www.hindawi.com/journals/tswj/2014/416530/abs/, 2014.

240

241   Chen, S., Zhang, J., Zhang, C., Yue, Q., Li, Y., & Li, C.: Equilibrium and kinetic studies
242   of
243   methyl orange and methyl violet adsorption on activated carbon derived from
244   Phragmites australis, Desalination, 252(1-3), 149-156,
245   https://www.sciencedirect.com/science/article/pii/S0011916409012193, 2010.

246

247   Daneshvar, N., Rasoulifard, M., Khataee, A., & Hosseinzadeh, F.: Removal of CI Acid
248   Orange 7 from aqueous solution by UV irradiation in the presence of ZnO
249   nanopowder, Journal of Hazardous Materials, 143(1-2), 95-101,
250   https://www.sciencedirect.com/science/article/pii/S0304389406010405, 2007.

251

252   Dai, K. Lu, L. Liang C., "Graphene oxide modiied ZnO nanorods hybrid with high
253   reusable photocatalytic activity under UV-LED irradiation," Materials Chemistry and
254   Physics, vol. 143, no. 3, pp. 1410–1416, 2014.

255

256   Jiang, R., Fu, Y. Q., Zhu, H. Y., Yao, J., & Xiao, L.: Removal of methyl orange from
257   aqueous solutions by magnetic maghemite/chitosan nanocomposite films: adsorption
258   kinetics and equilibrium, Journal of Applied Polymer Science, 125(S2), E540-E549,
259   https://onlinelibrary.wiley.com/doi/abs/10.1002/app.37003, 2012.

260

261   Karunakaran, C., Senthilvelan, S., Karuthapandian, S., & Balaraman, K.:
262   Photooxidation of
263   iodide ion on some semiconductor and non-semiconductor surfaces, Catalysis

264   Communications, 5(6), 283-290,
265   https://www.sciencedirect.com/science/article/pii/S1566736704000470, 2004.
266
267   Khataee, A., & Kasiri, M. B.: Photocatalytic degradation of organic dyes in the presence
268   of
269   nanostructured titanium dioxide: influence of the chemical structure of dyes, Journal
270   of Molecular Catalysis A: Chemical, 328(1-2), 8-26,
271   https://www.sciencedirect.com/science/article/pii/S1381116910002384, 2010.
272
273   Khataee, A., Pons, M.N., & Zahraa, O.: Photocatalytic degradation of three azo dyes
274   using
275   immobilized TiO2 nanoparticles on glass plates activated by UV light irradiation:
276   Influence of dye molecular structure, Journal of Hazardous Materials, 168(1), 451-
277   457, https://www.sciencedirect.com/science/article/pii/S0304389409002519, 2009.
278
279   Khodja, A. A., Sehili, T., Pilichowski, J.-F., & Boule, P.: Photocatalytic degradation of
280   2-
281   phenylphenol on TiO2 and ZnO in aqueous suspensions, Journal of Photochemistry
282   and   Photobiology   A: Chemistry,   141(2-3),   231-239,
283   https://www.sciencedirect.com/science/article/abs/pii/S1010603001004233, 2001.
284
285   Lazar, M., Varghese, S., & Nair, S.: Photocatalytic water treatment by titanium dioxide:
286   recent   updates,   Catalysts,   2(4),   572-601,   https://www.mdpi.com/2073-
287   4344/2/4/572/htm, 2012.
288
289   Liu, B., Zhao, X., Terashima, C., Fujishima, A., & Nakata, K.: Thermodynamic and
290   kinetic analysis of heterogeneous photocatalysis for semiconductor systems, Physical
291   Chemistry Chemical Physics, 16(19), 8751-8760,
292   https://pubs.rsc.org/en/content/articlelanding/2014/cp/c3cp55317e/unauth#!divAbstra
293   ct, 2014.
294
295   Liu,I. Hon, M. and Teoh, L. "hepreparation, characterization and photocatalytic activity
296   of radical-shaped CeO2 /ZnO microstructures," Ceramics International,vol.40,
297   no.3,pp.4019–4024,2014.
298
299   Mittal, A., Malviya, A., Kaur, D., Mittal, J., & Kurup, L.: Studies on the adsorption
300   kinetics
301   and isotherms for the removal and recovery of Methyl Orange from wastewaters using
302   waste materials, Journal of Hazardous Materials, 148(1-2), 229-240,
303   https://www.sciencedirect.com/science/article/pii/S0304389407002518, 2007.
304

305 Pandey, A., Kalal, S., Ameta, C., Ameta, R., Kumar, S., & Punjabi, P. B.: Synthesis,
306 characterization and application of naïve and nano-sized titanium dioxide as a
307 photocatalyst for degradation of methylene blue, Journal of Saudi Chemical Society,
308 19(5),  528-536,
309 https://www.sciencedirect.com/science/article/pii/S1319610315000678, 2015.

311 Pant, H. Park, C. Pant, P. Tijing, L. Kim, H. and Kim, C. "Synthesis, characterization,
312 and photocatalytic properties of ZnO nano-lower containing TiO2 NPs,"Ceramics
313 International,vol.38,no.4,pp.2943–2950,2012.

316 Ramli, C., Amali, Z., Asim, N., Isahak, W. N., Emdadi, Z., Ahmad-Ludin, N., Yarmo,
317 M. A., & Sopian, K.: Photocatalytic Degradation of Methylene Blue under UV Light
318 Irradiation on Prepared Carbonaceous, The Scientific World Journal, 2014,
319 https://www.hindawi.com/journals/tswj/2014/415136/abs/, 2014.

321 Ruiz, A. M., Sakai, G., Cornet, A., Shimanoe, K., Morante, J. R., & Yamazoe, N.:
322 Microstructure control of thermally stable TiO2 obtained by hydrothermal process for
323 gas sensors, Sensors and Actuators B: Chemical, 103(1-2), 312-317,
324 https://www.sciencedirect.com/science/article/pii/S0925400504002503, 2004. 282

326 Samadi, M. Pourjavadi, A. and Moshfegh, A. "Role of CdO addition on the growth and
327 photocatalytic activity of electrospun ZnO nanoibers: UV vs. visible light," Applied
328 Surface Science , vol. 298, pp. 147–154, 2014.

330 Sandberg, R. G., Henderson, G. H., White, R. D., & Eyring, E. M.: Kinetics of acid
331 dissociation-ion recombination of aqueous methyl orange, The Journal of Physical
332 Chemistry,  76(26),  4023-4025,
333 https://pubs.acs.org/doi/abs/10.1021/j100670a024?journalCode=jpchax, 1972.

335 [Uddin, M. Nicolas, Y. Olivier Cl., "Nanostructured SnO2-ZnO heterojunction
336 photocatalysts showing enhanced photocatalytic activity for the degradation of organic
337 dyes," Inorganic Chemistry ,vol.51,no.14,pp.7764–7773,2012.

339 Xiao, Y., Lu, L., Zhang, A., Zhang, Y., Sun, L., Huo, L., & Li, F.: Highly enhanced
340 acetone sensing performances of porous and single crystalline ZnO nanosheets: high
341 percentage of exposed (100) facets working together with surface modification with
342 Pd nanoparticles, ACS applied materials & interfaces, 4(8), 3797-3804,
343 https://pubs.acs.org/doi/abs/10.1021/am3010303, 2012.
344

345   Xu, C., Rangaiah, G., & Zhao, X.: Photocatalytic degradation of methylene blue by
346   titanium
347   dioxide: experimental and modeling study, Industrial & Engineering Chemistry
348   Research, 53(38), 14641-14649, https://pubs.acs.org/doi/abs/10.1021/ie502367x,
349   2014.
350
351   Zhou, X. Shi, T. and Zhou, H. "Hydrothermal preparation of ZnO-reduced graphene
352   oxide hybrid with high performance in photocatalytic degradation," Applied Surface
353   Science,vol.258,
354   no. 17, pp. 6204–6211, 2012.
355
356
357
358
359
360
361
362
363
364
365
366
367
368
369
370
371
372
373
374
375
376
377
378

379
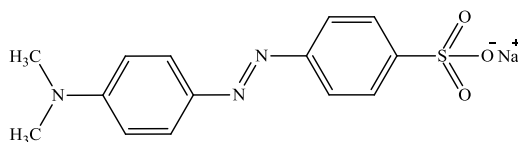
Fig. 1.The chemical structure of methyl orange.

380

381

382

383

384

385

386

387

388

389

390

391

392

393

394

395

396

397

398

399

400

401

402

403

404

405

406

407

408

409

410

411

412   Fig. 2. The photo-catalytic time vs absorbance without SL.
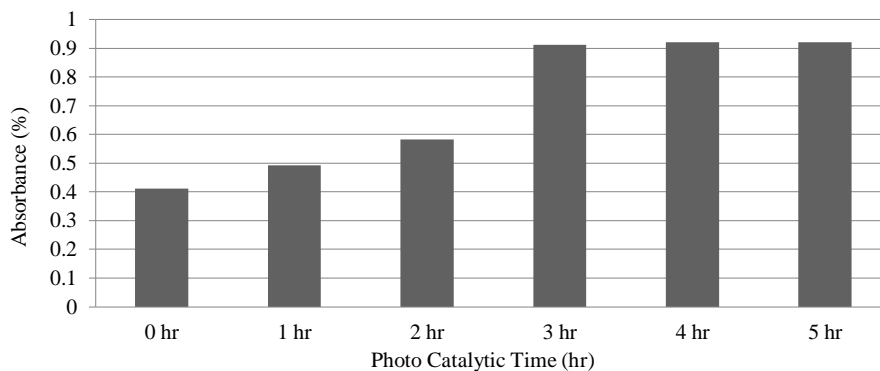
413

414

415

416

417

418

419

420

421

422

423

424

425

426

427

428

429

430

431

432

433

434

435

436

437

Fig. 3. UV–visible spectra of Er_2O_3 nanoparticles without SL.
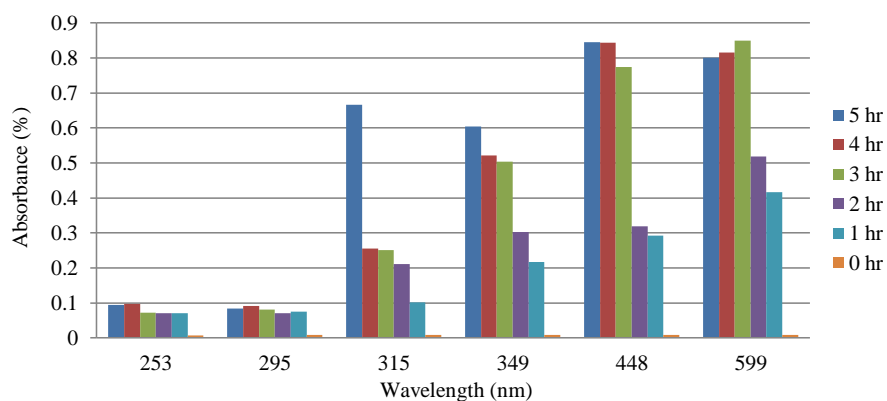
438

439

440

441

442

443

444

445

446

447

448

449

450

451

452

453
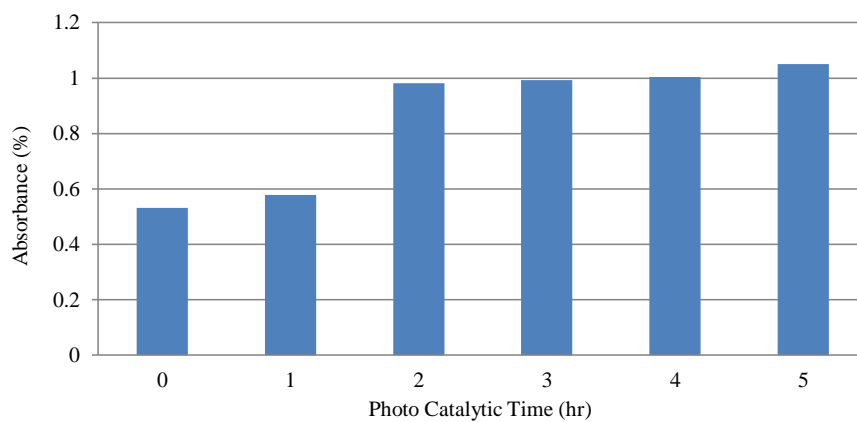
Fig. 4. Photo-catalytic degradation of methylene blue dye over Er_2O_3 samples as a function of
irradiation time with SL.

456

457

458

459

460

461

462

463

464

465

466

467

468

469

470

471

472

473

474

475

476

Fig. 5. UV–visible spectra of Er$_2$O$_3$ with SL.
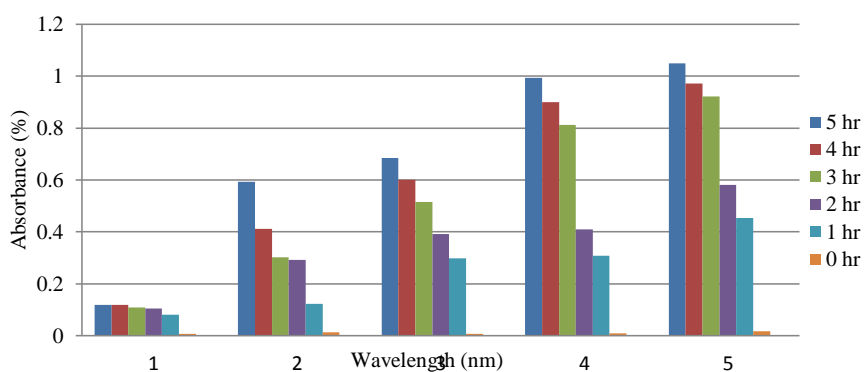
477

478

479

480

481

482

483

484

485

486

487

488

489

490

491

492

493

494

495

Fig. 6. The concentration of MO dye versus with absorbance, with and without irradiation.
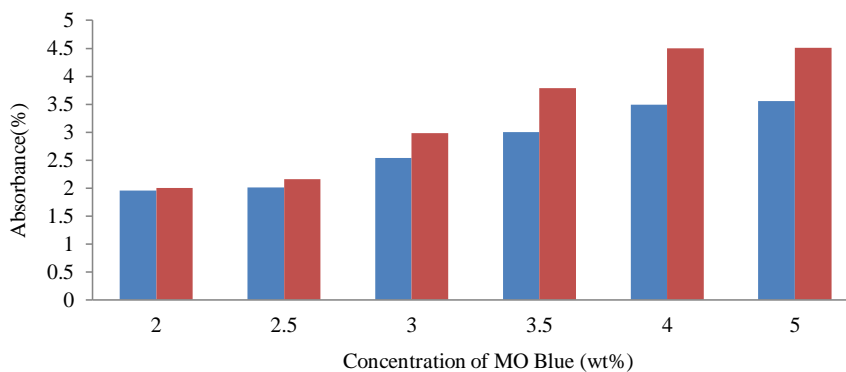
497

498

499

500

501

502

503

504

505

506

507

508

509

510

511
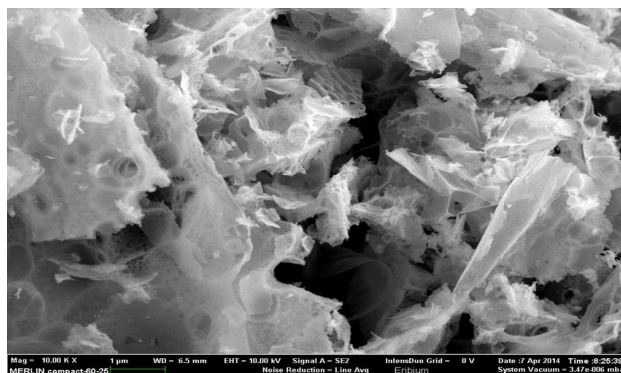
512   Fig. 7. SEM image shows a distribution of Erbium oxide particles 1000 kx.

513

514

515

516

517

518

519

520

521

522

523

524

525

526

527

528

529

530

531
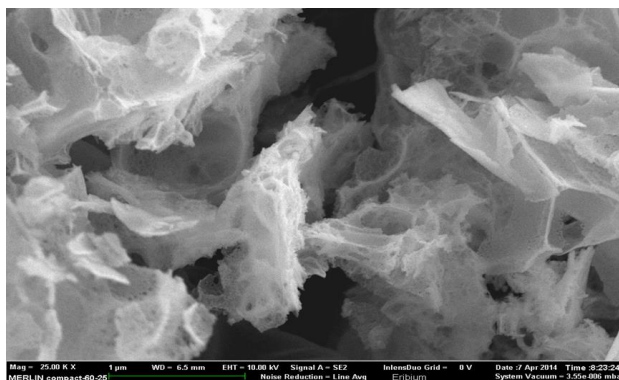
532   Fig. 8. Shows an even distribution for Erbium oxide particles 2500 kx.

533

534

535

536

537

538

539

540

541

542

543

544

545

546

547

548

549
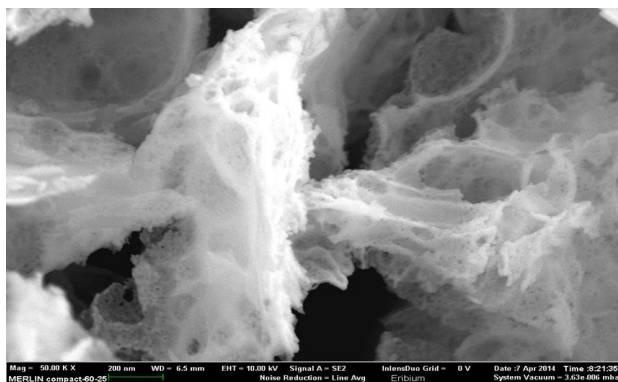
Fig. 9. SEM image of nano-sized Er_2O_3 5000 kx.

550

551

552

553

554

555

556

557

558

559

560

561

562

563

564

565

566

567
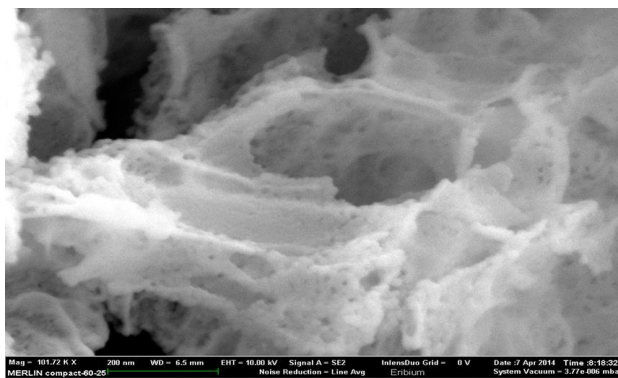
568   Fig. 10. SEM image of nanosized Er$_2$O$_3$ 101.72 kx.

569

570

571

572

573

574

575

576

577

578

579

580

581

582

583

584

585

586
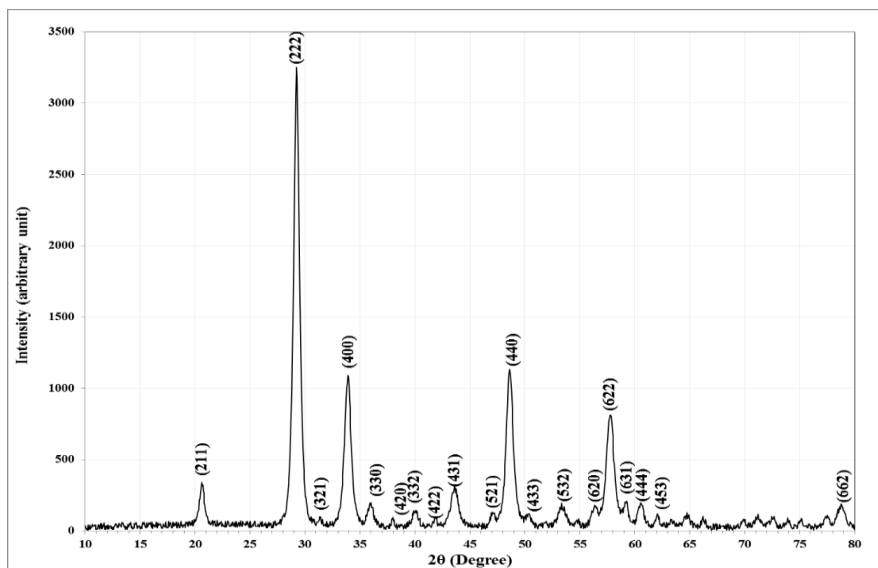
587

588

Fig. 11. XRD of Er_2O_3 nanoparticles.

589

590

591

592

593

594

595

596

597

598

599

600

601

602

603   Table 1. XRD parameter of Er_2O_3 nanoparticles.

2Θ (Deg.)	FWHM (Deg.)	d_{hk1} Exp. (A)	G.S. (nm)	Hk1	d_{hk1} Std. (A)	Phase	Card No.	δ
20.6330	0.4972	4.3013	16.2	(211)	4.3029	Cub.Er_2O_3	96-101-0593	0.0004
29.2389	0.6119	3.0519	13.4	(222)	3.0426	Cub.Er_2O_3	96-101-0593	0.0031
31.4191	0.3060	2.8449	27.0	(321)	2.8169	Cub.Er_2O_3	96-101-0593	0.0100
33.9052	0.6884	2.6418	12.1	(400)	2.6350	Cub.Er_2O_3	96-101-0593	0.0026
35.9706	0.6120	2.4947	13.7	(330)	2.4843	Cub.Er_2O_3	96-101-0593	0.0042
37.9978	0.2677	2.3661	31.4	(420)	2.3568	Cub.Er_2O_3	96-101-0593	0.0040
40.0249	0.6119	2.2509	13.8	(332)	2.2471	Cub.Er_2O_3	96-101-0593	0.0017
43.6203	0.8032	2.0733	10.7	(431)	2.0671	Cub.Er_2O_3	96-101-0593	0.0030
47.0626	0.4208	1.9294	20.6	(521)	1.9243	Cub.Er_2O_3	96-101-0593	0.0026
48.6308	0.7267	1.8708	12.0	(440)	1.8632	Cub.Er_2O_3	96-101-0593	0.0041
50.3137	0.5737	1.8121	15.3	(433)	1.8076	Cub.Er_2O_3	96-101-0593	0.0025
53.3736	0.7650	1.7152	11.6	(532)	1.7098	Cub.Er_2O_3	96-101-0593	0.0031
56.3187	0.6120	1.6322	14.7	(620)	1.6665	Cub.Er_2O_3	96-101-0593	0.0206
57.7722	0.8032	1.5946	11.3	(622)	1.5890	Cub.Er_2O_3	96-101-0593	0.0035
59.1874	0.4972	1.5598	18.4	(631)	1.5540	Cub.Er_2O_3	96-101-0593	0.0037
60.5643	0.6120	1.5276	15.0	(444)	1.5213	Cub.Er_2O_3	96-101-0593	0.0041
62.0560	0.4590	1.4944	20.2	(543)	1.4906	Cub.Er_2O_3	96-101-0593	0.0026
78.7705	0.8032	1.2140	12.8	(662)	1.2090	Cub.Er_2O_3	96-101-0593	0.0041

604